Improved potential energy surface and spectral assignments for ammonia in the near-infrared region

Phillip A. Coles[a], Roman I. Ovsyannikov[b], Oleg L. Polyansky[a,b], Sergei N. Yurchenko[a], Jonathan Tennyson[a,*]

[a] *Department of Physics and Astronomy, University College London, London WC1E 6BT, UK*
[b] *Institute of Applied Physics, Russian Academy of Sciences, Ulyanov Street 46, Nizhny Novgorod 603950, Russia*

A B S T R A C T

A new 'spectroscopic' potential energy surface (PES) for $^{14}NH_3$ has been generated by refinement of a high accuracy *ab initio* PES to experimental data. The quality of the PES is reflected in the excellent agreement between calculated rovibrational energy levels and the empirical values of MARVEL. The PES is used in conjunction with two different DMSs to generate room temperature line lists up to 12 000 and 20 000 cm^{-1}, including all transitions from lower states up to 4000 cm^{-1}, with total angular momentum up to $J = 20$. Several strong bands are found to be missing from HITRAN 2016 in the 5700–6200 cm^{-1} region. Using the line lists, 769 transitions in the 7400–8000 cm^{-1} are assigned by ground state combination difference (GSCDs), along with empirical upper state energies and full quantum labels for 284 levels. 53 of our assignments were found to disagree with those given in HITRAN 2016.

1. Introduction

Ammonia (NH_3) spectra are of both fundamental interest and of practical importance. Ammonia is the classic example of a system undergoing tunneling which remains a subject of ongoing studies [1]. Ammonia production has more than doubled during the period of industrialisation [2] and is probably the most abundant man-made gas in the world. Ammonia is emitted from livestock, fertilizers and fuel burning, and contributes to acid decomposition and eutrophication which may harm natural ecosystems [3]. Additionally there is mounting evidence indicating ammonia is critical in the formation of secondary aerosols, which have a harmful impact on human health [3].

For these reasons NH_3 atmospheric emissions must be closely monitored by *in situ* detectors, which rely on accurate knowledge of line positions, intensities, temperature dependence, pressure broadening etc. Some of this information is provided by spectroscopic databases [4,5], but there are large gaps in the coverage. Al Derzi et al. [6] give a comprehensive review of high resolution spectroscopic data recorded and analysed up to 2014. Spectroscopic data is particularly missing in the near infrared, including the so-called telecoms region at 1.3 and 1.5 μm, which provides a

good window for monitoring ammonia concentrations because of the reduced interference from water vapour and the availability of cheap diodes in this region [7–9].

So far the main provider of information of the near infrared spectrum of ammonia has been theoretical line lists computed with variational nuclear motion programs [10–13]. In this context the important line lists are BYTe [11] and HSL-pre3 [14,15]. BYTe is a variationally computed line list for $^{14}NH_3$ covering transitions from 0 to 12 000 cm^{-1} and temperatures up to 1500 K. The 'spectroscopic' potential energy surface (PES), named NH3-Y2010 [16], used to construct BYTe was produced by empirical refinement of a high quality *ab initio* surface to experimental data. The resulting accuracy varies, but is typically sub-wavenumber for energies under 6000 cm^{-1}, and as much as several wavenumbers thereafter. HSL-pre3 [14], the successor to HSL-2 [12], provides a more accurate list of rovibrational energies and transition frequencies. However, no intensities or complete vibrational labels are included, making it unsuitable for assignment in many cases. Finally, it is worth mentioning the recent high accuracy *ab initio* PES of Polyansky et al. [17]. The accuracy of their calculated band centres pushes the boundaries of what is achievable purely *ab initio*. However, their reported accuracy for energies up to 18 000 cm^{-1} can be reached only using a very large rotation-vibration basis set that becomes computationally unmanageable for $J \gg 0$ calculations.

Alongside these advancements in theory over the past 10 years, have come the first serious attempts at wide-scale characterisation of NH_3 above $5000\,cm^{-1}$. Several notable works in the 1.5 µm region being those of Xu, Lees and co-workers [18–20], and Sung et al. [14]. In just the past 3 years there has been considerable progress above $7000\,cm^{-1}$, largely due to the discovery, and subsequent analysis of the 1980 high resolution Kitt Peak spectrum by Barton et al. [21,22] and Zobov et al. [23]. In particular, Barton et al. assigned over 3000 transitions spanning 27 vibrational bands in the 7400–$9900\,cm^{-1}$ range employing a method using BYTe, combination differences and the method of branches [24]. Their line lists and quantum assignments were included in the HITRAN 2016 database. Even so, many strong lines remain unassigned due to the inaccuracy of BYTe line positions, and so more accurate variational calculations are highly desirable. Barton et al. [22] also made partial assignments of the strong bands lying in the 9000–9400 and 9900–$10\,300\,cm^{-1}$ regions. More recently, Zobov et al. [23] used the *ab initio* PES of Polyansky et al. in conjunction with the rovibrational calculations presented here to analyse red and green visible spectra recorded at Kitt Peak in the $15\,500$ and $18\,000\,cm^{-1}$ regions. They assigned transitions within the 5 and 6 quanta N-H stretching overtones in these spectra as well as transitions observed in the 1980s by Coy and Lehmann [25–27].

In this paper we present a new spectroscopic PES and room temperature line list calculations to aid analysis of the rapidly growing experimental dataset of ammonia; we use these results to re-analyse some of the spectra of NH_3 available in the literature. Section 2 outlines our refinement procedure, including the general methodology and computational details (2.1), experimental data included in the refinement (2.2) and our final refined parameters (2.3). Section 3 presents our results, including structural constants of our PES (3.1), a comparison of our calculated rovibrational energies to high accuracy experimental values (3.2), intensity calculations (3.3), and new assignments (3.4). In Section 4 we conclude.

2. Potential energy surface refinement

2.1. Computational details

Our general strategy is based on the one used to construct the NH3-Y2010 PES [16]; in this work the refinement is represented by a correction potential ΔV which is added to the starting PES. Our starting point PES was the high accuracy *ab initio* surface of Polyansky et al. [17]. In their nuclear motion calculations Polyansky et al. employed a version of TROVE specifically adapted to use curvilinear coordinates [28] in conjunction with a large basis set constrained by a maximum polyad (P_{max}) of 40. The polyad number in general represents our total vibrational quanta in terms of the lowest energy harmonics, and in the case of NH_3 is defined as

$$P = 2(n_1 + n_2 + n_3) + n_4 + n_5 + \frac{n_6}{2}, \tag{1}$$

where n_i are local mode quantum numbers representing the stretch ($i = 1, 2, 3$), degenerate bend ($i = 4, 5$) and inversion ($i = 6$) of the primitive basis set functions as constructed and used by TROVE. The stretching and inversion basis functions are generated using the Numerov-Cooley approach [29–31], while for the asymmetric bending modes harmonic oscillators are used. This basis set is processed through a two-step contraction-symmetrisation technique [32]. The final, contracted vibrational ($J = 0$) basis set used in the refinement comprised all eigenfunctions of the $J = 0$ Hamiltonian which correspond to the energies below $hc \cdot 20\,000\,cm^{-1}$. The rotational basis functions are symmetrized combinations of spherical harmonics as described previously [33].

Owing to the computer resources available to us we were limited to using $P_{max} = 34$, therefore all rovibrational calculations reported in this work were performed using a $P_{max} = 34$ basis set. The most computationally expensive step necessary for the refinement procedure is the generation and symmetrisation of the Hamiltonian matrix elements of each term in the correction potential. This is required in order to calculate the Hellmann–Feynman derivatives that constitute the Jacobian matrix necessary for the least-squares fitting, and is the primary factor that limits our basis set size. At $P_{max} = 34$ this process requires 54 Gb of RAM per correctional term. Ideally, we would pick a value of P_{max} such that our vibrational eigenfunctions are converged for at least all energies up to the highest value included in the refinement. However, our convergence testing indicates a P_{max} of 34 provides eigenvalues converged to $< 0.1\,cm^{-1}$ only up to about $8000\,cm^{-1}$, compared to the highest experimental energy included in the refinement being $\sim 18\,000\,cm^{-1}$. In this case the error due to using an incomplete basis set is absorbed into the refined potential.

TROVE employs a Taylor-type expansion of the kinetic energy operator and a re-expansion of the potential function in terms of linearized coordinates, which we take to 6th and 8th order respectively. The effect of this has been documented in the past [17], and is typically less than $0.1\,cm^{-1}$ for energies under $10\,000\,cm^{-1}$. All of the aforementioned choices contribute somewhat to the reproducibility of our results using other nuclear motion programs, meaning our results at higher energies are only reproducible using TROVE with a specific set of model input parameters. Nevertheless, with a converged basis set we expect the only source of variation between programs to be our expansion of the Hamiltonian.

At lower energies we tested the reproducibility of our results by comparing TROVE calculations with ones performed using the nuclear motion program GENIUSH [34], which uses an exact kinetic energy operator and a discrete variable representation (DVR). Comparisons of the 16 lowest lying vibrational term values calculated using TROVE and GENIUSH and our refined potential in absence of the Born-Oppenheimer diagonal correction (BODC) show small discrepancies no greater than $0.281\,cm^{-1}$. We attribute this to (*i*) our truncation of the kinetic energy operator expansion after 6th order; and (*ii*) our re-expansion of the potential in terms of linearised coordinates.

2.2. Experimental data and weights included in the refinement

The complete list of experimental energies used in the refinement is included in the supplementary material. Our primary source of experimental data was the MARVEL (measured active rotation-vibration energy levels) [35] study of ammonia by Al Derzi et al. [6], which contains the most accurate and most complete list of experimentally-derived energies available for NH_3. From this source we initially included 543 carefully selected states ranging from 0 – $7254\,cm^{-1}$ with $J \leq 8$. Because the quality of the refinement depends crucially on the accuracy of the experimental data, we assessed the reliability of each MARVEL state prior to the refinement based on the number of transitions it was involved in, and whether it followed the expected $J - K$ dependence within the vibrational band. During the refinement, any states that did not behave similarly to the rest of the band were removed, as they tended to degrade the quality of the refinement. In total we identified 81 MARVEL states with $J \leq 15$ for which no suitable partner could be found in our calculated energies list, and a further 80 that displayed uncomfortably large residuals of between 0.5 and $4.0\,cm^{-1}$. There has been a recent update of the $^{14}NH_3$ MARVEL energy levels [36] which used energy levels computed from intermediate version of our refined PES, in conjunction with the BYTe and HSL-pre3 energies lists to validate states

below 7555 cm^{-1} . As a result of this work, these discrepancies have been largely resolved and we were able to include an additional 94 energies from this updated MARVEL dataset in our fits.

Between 7555 cm^{-1} and 11 000 cm^{-1} the only existing experimental assignments are those of Barton et al. [21,22]. Due to the complexity of spectra in this region only some of their assignments could be confirmed by ground state combination differences (GSCDs), and in this case there is always the possibility of mis-assignment. Even if a GSCD partner is found, such dense spectra will contain false positives that fall within the tolerance ranges of the assignment. This is especially true if the line positions and intensities of the *ab initio* calculations are of dubious accuracy, and the particular GSCD partner is a medium strength or weak line. We therefore decided to take a cautious approach, preferring to use only 34 energies from the $\nu_2 + 2\nu_3$ band of Barton et al. [21], which we found to be reliable, and perform our own tentative assignments using the *ab initio* PES of Polyansky et al. [17] and intermediate versions of the refinement. This provided 105 additional energies ranging from 7584 to 10512 cm^{-1}, although most of these levels were derived from only one experimental transition via a visual comparison between line lists.

It is well known that the inclusion of $J > 0$ states in the refinement is necessary to optimise the equilibrium geometry [37], and it is preferable for each J to contain K sublevels ranging from $0 - J$ to constrain both the B_e and C_e oblate top rotational constants. We included states with $J = 0 - 4, 6, 8$ in the refinement, however, to save on computational costs only A_2' and A_2'' were used for $J > 3$. Enough experimental data fell within these criteria to provide sampling of all important normal mode directions along our PES. Several high energy band centers at 12 000, 15 000 and 18 000 cm^{-1} were also included from the early work of Coy and Lehmann [27] which, at the time of performing our calculations, were the only assigned spectra above 12 000 cm^{-1} available in the literature. We also note the unassigned $5\nu_1$ absorption bands of NH$_3$ by Giver et al. [38].

As high energy data is scarce it is possible for the refined PES to assume unphysical shapes far from equilibrium. We therefore constrained the refinement to the original, low-weighted *ab initio* points following the simultaneous fit approach by Yurchenko et al. [39], with the motivation that our refined surface not deviate substantially from the *ab initio* surface. Initially these consisted of the same 20 000 points between 0 and 20 000 cm^{-1} that were used to fit the *ab initio* PES [17], but we had problems with holes and double minima appearing above 20 000 cm^{-1} but below dissociation at 40 000 cm^{-1}. To prevent this, a further 13 000 points were generated between 20 000 and 50 000 cm^{-1} using the *ab initio* PES, and included in the refinement. The energy-dependent scheme of Ref. [17] was used to allocate weights below dissociation, and a constant value of 0.00065 was used above. All *ab initio* point weights were then multiplied by a constant factor that started at 1×10^{-4} and was gradually decreased to 1×10^{-7} as the refinement progressed.

We used the weighting scheme $w_i \sim 1/\sigma_i^2$ for all MARVEL states, where σ_i is the standard error of the ith energy level, as this information is provided in the MARVEL database. This is known to be the optimum weighting structure for a general least-squares fit. For states derived from the Kitt Peak spectrum, weights were distributed uniformly, with a slight energy dependence to reduce the importance of very high energy states. On the last five iterations of the Newton-Gauss algorithm, once improvements with each iteration began to stagnate, the weights were changed so that each energy $E^{J, \Gamma}$ had a weight of J, and $J = 0$ had a weight of 1. This served to improve the fit for those bands containing fewer, or less accurately known, experimental energies. The robust weighting method by Watson [40] was used to adjust the fitting weights on-the-fly.

2.3. Refined parameters

We call our refined potential NH3-C2018. Refined potential parameters are included as supplementary material in the form of a Fortran subroutine. The refined potential is represented as a sixth order polynomial as described by Polyansky et al. [17], where the refined parameters $f_{ijk\ldots}^{(s)}$ are the expansion coefficients of Morse-type stretching ($i = 1, 2, 3$) and symmetrised bending ($i = 4, 5$) coordinates. We could usefully vary 176 parameters up to fifth order in the refinement, excluding the Born-Oppenheimer diagonal correction term due to Polyansky et al. [17] which we kept fixed. Variation of linear terms allowed us to simulate the effects of optimising the equilibrium geometry without resorting to a separate Newton-Gauss style procedure, which cannot be performed concurrently with the PES refinement, and severely changes the vibrational structure.

Refined parameters higher than second order generally differed quite substantially from their starting value. However, the harmonic terms remained consistent, with the zero-order-inversion stretching and bending terms ($f_{11}^{(0)}$ and $f_{44}^{(0)}$) changing only by 0.45% and 0.06% respectively. Coupling terms $f_{12}^{(0)}$ and $f_{14}^{(0)}$ showed larger changes of 10.7% and 2.3%, and harmonic terms that were first order in the inversion coordinate $f_{11}^{(1)}$, $f_{44}^{(1)}$, $f_{12}^{(1)}$ and $f_{14}^{(1)}$ changed by 17%, 21%, 11% and 2% respectively. This level of change in the low-order parameters is acceptable, and the apparent instability of higher-order parameters is not too worrying; in truth there are a large number of possible combinations that can produce similarly shaped potentials. Most importantly, the energy difference between the refined and *ab initio* PESs is always less than 10% that of the *ab initio* PES above its zero-point energy (ZPE) for grid points under 50 000 cm^{-1} . This was confirmed by evaluating both PESs on a random grid of 50 000 points with borders at $0.6 \leq r_1 \leq r_2 \leq r_3 \leq 1.58$ Å and $30° \leq \alpha_1 \leq \alpha_2 \leq \alpha_3 \leq 140°$. Further reassurance that our PES does not suffer from any unphysical deformities is provided by the GENIUSH [34] calculations given in Section 2.1, for which a large grid of one million points was used. By nature of the DVR approach, any deep holes that exist within the grid borders are manifested in the zero point energy, which was seen to take unreasonable values if holes were present.

3. Results and discussion

3.1. Equilibrium structure and rotational energies

The various structural parameters of our PES NH3-C2018 are given in Table 1, along with other theoretically predicted and experimentally derived values. Our equilibrium structure is very similar to that predicted by the NH3-Y2010 and HSL-2 PESs, with our bond angle, α_{eq}, slightly larger than both, and our bond length, r_{eq}, roughly half way between the two. Pure rotational energies are highly sensitive to changes in equilibrium geometry, and so accurate rotational energies are therefore indicative of an accurate equilibrium geometry.

Table 2 compares our rotational energies to those of MARVEL for states up to $J = 30$. For $J = 0 - 10$ our predictions show excellent agreement with the empirical values. The small differences of order 0.001 cm^{-1} are likely to be inside the values which are determined due to beyond Born-Oppenheimer (BO) effects. As J increases, the agreement deteriorates, and beyond $J = 20$ significant discrepancies appear. These are as much as several wavenumbers for $J = 30$ states with large K values, and as K decreases the agreement rapidly improves. Intuitively this can be explained by the centrifugal force flattening and stretching the molecule, which will

Table 1
Structural constants of our PES compared to previous theoretical calculations and experiment.

	NH3-C2018	NH3-Y2010 [16]	HSL-2 [12]	Exp[41].	Exp[42].	Exp[43].
r_{eq} /Å	1.010794	1.0109285	1.010668	1.01101	1.01139	1.0116
α_{eq} /°	106.7894	106.7468	106.7489	106.75	107.17	106.68
r_{SP} /Å	0.993882	0.9943827	0.9942537	0.99460		
ΔE(barrier) / cm^{-1}	1775.17	1766.83	1784.66	1786.8		

Table 2
Accuracy of calculated rotational energy levels up to $J = 30$ when compared to the empirical MARVEL energies [6]. σ_{rms} refers to the root-mean-square deviation and Δ refers to the $E_{MARV} - E_{calc}$ energy differences of $K = J$ and $K = 0$ states. Units are cm^{-1}.

J	σ_{rms}	$\Delta(K = J)$	$\Delta(K = 0)$
0	0.001		
1	0.001	−0.001	0.000
2	0.001	−0.002	0.000
3	0.001	−0.002	0.001
4	0.001	−0.002	0.001
5	0.001	−0.002	0.002
6	0.002	−0.002	0.003
7	0.001	−0.001	0.003
8	0.001	0.001	0.003
9	0.002	0.002	0.003
10	0.004	0.002	0.005
11	0.006	0.002	0.009
12	0.009	−0.001	0.015
13	0.014	−0.004	0.020
14	0.018	−0.011	0.029
15	0.026	−0.024	0.038
20	0.176	−0.576	0.130
30	3.322	−11.353	0.546

be more distorting for rotation about the primary axis. Both the inversion and stretching potentials therefore strongly couple to the equilibrium geometry at high rotational excitation.

Almost identical systematic deviations exist with the BYTe line list, for which the $J = 30$ rotational energies differ from our calculations by at most 0.1 cm^{-1}. This may suggest both PESs share a similar systematic offset in the inversion potential at high energies. One solution would be to include higher order ν_2 overtones in the refinement, however, in order to sample the same energetic region as a $(J, K) = (30, 0)$ rotational state (~ 8600 cm^{-1}) we would require empirical energies from the $9\nu_2$ and $10\nu_2$ bands. Alternatively we may include very high J states in the refinement, which is extremely computationally demanding using the current procedure. For example, simply saving the necessary Jacobian matrices for a $J = 30, A_2'$ block would require 10s of Tb of disk space, which is far beyond our current computational resources.

3.2. Rovibrational calculations

Rovibrational energy level calculations were performed up to $J = 20$ using the NH3-C2018 PES in conjunction with the variational nuclear motion program TROVE [29], with its specific application to XY$_3$-type molecules given by Yurchenko et al. [33]. Basis set and Taylor series truncations were the same as discussed in Section 2.1 although this time we removed the energy cut-off in our vibrational basis set. The result is a huge increase in computational demand, but we found it necessary in order to converge all rotationally excited states belonging to the stretching overtones at 18 000 cm^{-1}. Our complete list of energies extends to 23 000 cm^{-1}, and is included in the supplementary material along with associated quantum labels (ν_1, ν_2, ν_3, L_3, ν_4, L_4, Γ_{vib}, J, K, i, Γ_{rot}, Γ_{tot}) and partnered MARVEL levels where available.

To assess the accuracy of our energies list we first compare with MARVEL energies under 7555 cm^{-1}. Beyond this, MARVEL data is solely derived from the works of Barton et al. [21], which we will discuss separately in Section 3.4. Fig. 1 displays $E_{MARV} - E_{calc}$ energy residuals for $J \leq 10$ states under 6300 cm^{-1} with BYTe residuals ($E_{MARV} - E_{BYTe}$) included for comparison. Table 3 provides the associated root-mean-square (rms) deviation statistics as a function of J and MARVEL vibrational label. Overall agreement is excellent, with our rms values σ_{rms} generally staying below 0.1 cm^{-1} except in a few cases which will be discussed below. Unlike BYTe, we do not utilise the empirical basis set correction (EBSC) [10], whereby the calculated vibrational band centres are replaced by their experimental counterparts. Despite this, all our vibrational term values below 6300 cm^{-1} fall within 0.01-0.04 cm^{-1} of the MARVEL empirical values. Similar accuracy is expected for the remaining band origins for which only $J > 0$ MARVEL data exists, with the only likely exception being the $(\nu_2 + 2\nu_4^2)^s$ band for which data were extremely limited. Whilst no experimentally derived band center could be found in the literature, we judge from our $J = 1$ comparisons that our predicted band center is roughly 0.1 cm^{-1} larger than the true value.

A relatively smooth increase in energy residuals with J is observed for most vibrational bands, and despite excluding states above $J = 8$ from the refinement the $J = 9, 10$ residuals behave in the same systematic way as those for $J = 0 - 8$. This speaks for the predictive power of the refinement, and reassures us that our calculations can safely be extended to higher rotational excitations. Larger increases in residuals are observed for the $2\nu_2 + \nu_3$ band, for which data only became available in the final stages of the refinement, and the $(\nu_1)^s$ band, for which the $J = 10$ rms error of 0.106 cm^{-1} (see Table 3) is still at least five times smaller than our predecessor BYTe. Note that below 6300 cm^{-1} there is little difference in rms errors between MARVEL states derived from 1 or 2 transitions and those derived from 3 or more. However, given the accuracy of our $J = 0 - 10$ calculations for the $2\nu_4^0$ and $2\nu_4^2$ bands it is possible that the MARVEL $J = 12$ energies, derived from only one transition, may not be correct.

Further suspicious energies are those belonging to the $2\nu_2 + \nu_4$, $2\nu_2 + 2\nu_4$ and $2\nu_2 + 3\nu_4$ bands. Inclusion of these bands in the refinement severely damaged the quality of surrounding energies, and so they were omitted. Comparing our predictions for the $2\nu_2 + \nu_4$ with HSL-pre3 we find slightly better agreement, and for the 14 $J = 0 - 8$ states present in MARVEL the rms deviation between NH3-C2018 and HSL-pre3 is only 0.272 cm^{-1}. Considering the general lack of experimental data assigned to these bands, it remains unclear whether this is a problem of theory or experiment.

Above 6300 cm^{-1} we noticed several labelling conflicts between our own calculations and those of HSL-pre3 and MARVEL (see Table 4) associated with the $\nu_1 + \nu_3$, $\nu_3 + 2\nu_4^2$ and $\nu_3 + 2\nu_4^0$ bands. For this reason we simply use the MARVEL labels for our comparisons in Fig. 2 and Table 3, and provide our own vibrational labels and band origins separately in Table 4. To avoid duplication of the $\nu_1 + \nu_3$ band center in our energies list, we suggest using the labels $(\nu_3 + 2\nu_4^0)^{s/a}$ for the 6608 and 6609 cm^{-1} vibrational term values so that our labelling scheme is identical to found in HSL-pre3. Sung et al. [44] also suggest a unique list of labels based
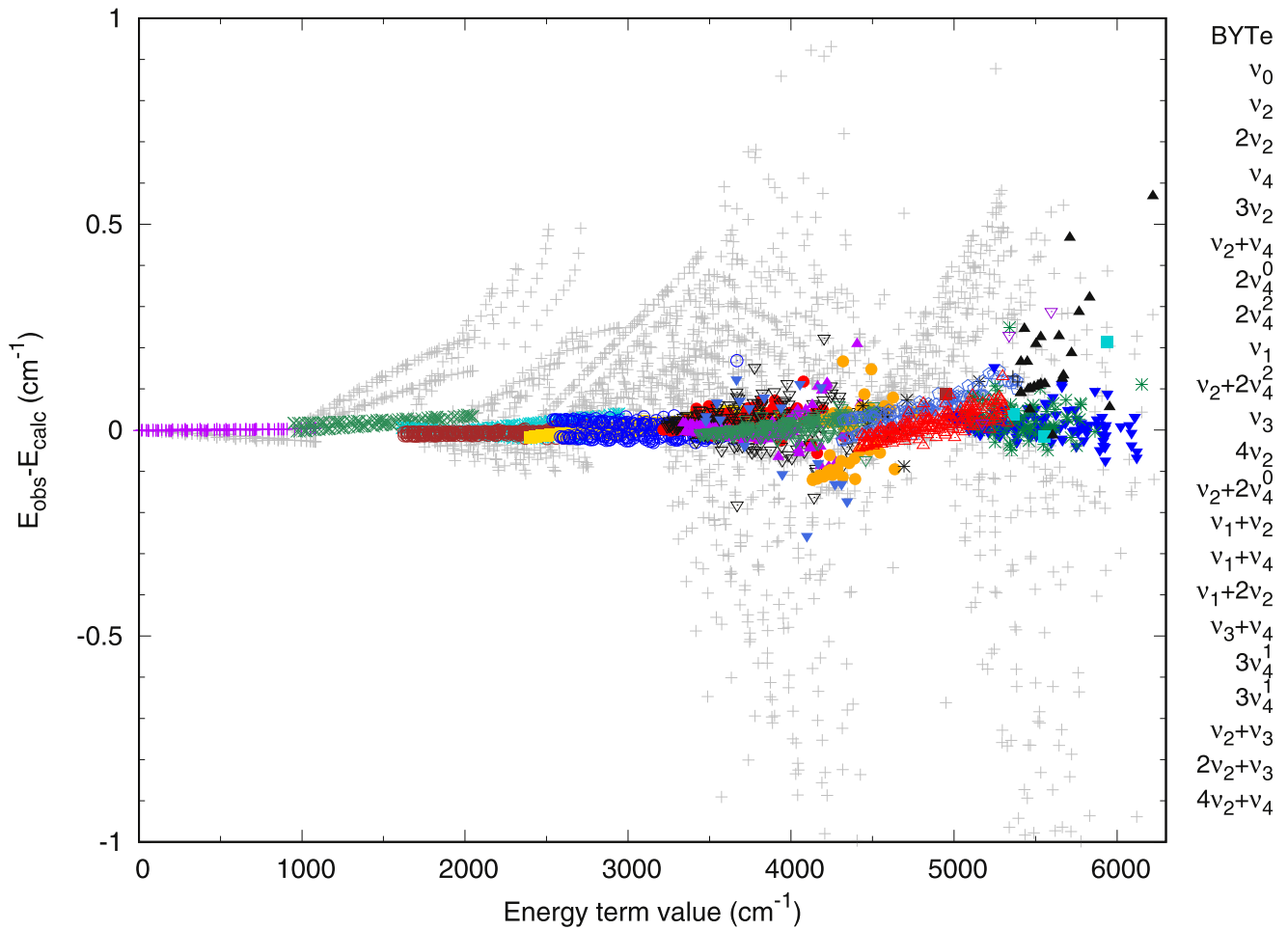
Fig. 1. Energy difference between $J = 0 - 10$ MARVEL energy levels under $6300\,cm^{-1}$ and those of NH3-C2018.
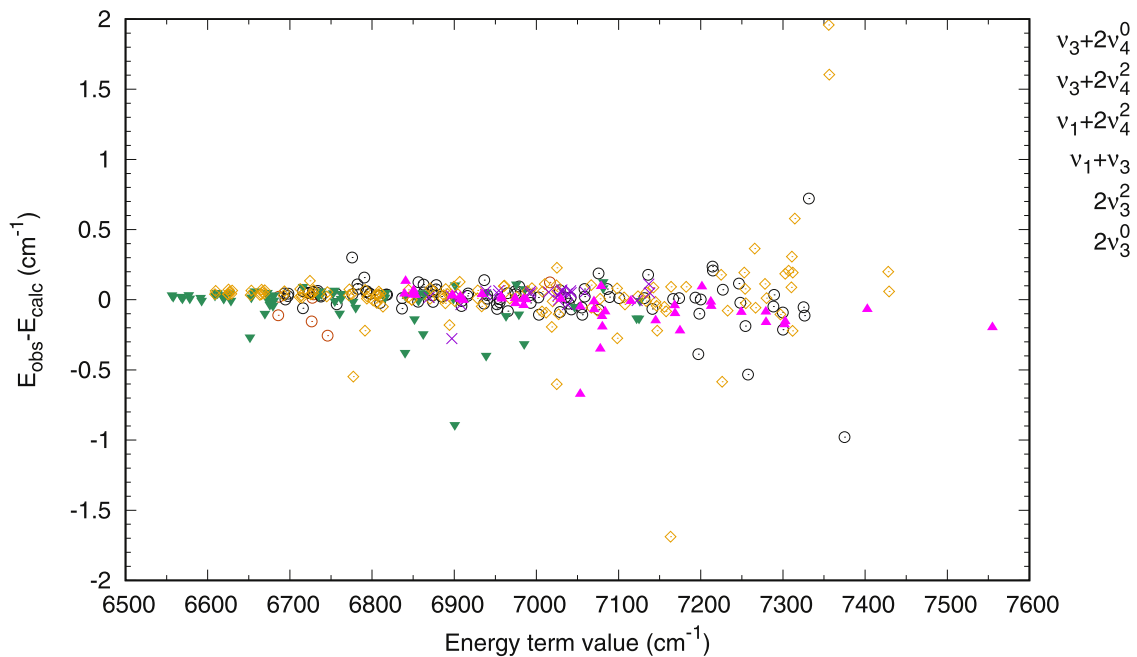

Fig. 2. Energy difference between $J = 0 - 10$ MARVEL energy levels above $6300\,cm^{-1}$ and those of NH3-C2018. Only MARVEL levels derived from 3 or more transitions are shown.

Table 3

Root-mean-square deviations statistics for the complete list of paired MARVEL-NH3-C2018 energies under 7555 cm^{-1}. N$_{states}$ refers to the number of paired states included in the comparison. The value before the / refers to all MARVEL states, and the value after the / refers to those states derived from 3 or more transitions. Vibrational labels are taken from MARVEL.

Band	Band center		$J = 1-8$		$J = 10$		$J = 12$	
	This work	MARVEL [6]	N$_{states}$	σ_{rms}	N$_{states}$	σ_{rms}	N$_{states}$	σ_{rms}
$(\nu_2)^s$	932.4170		40/40	0.021/0.021	10/10	0.030/0.030	12/12	0.039/0.039
$(\nu_2)^a$	968.1253	968.1266	40/40	0.010/0.010	11/11	0.027/0.027	13/13	0.041/0.041
$(2\nu_2)^s$	1597.4674		40/40	0.008/0.008	10/10	0.014/0.014	11/11	0.017/0.017
$(2\nu_2)^a$	1882.1847	1882.1774	40/40	0.012/0.012	11/11	0.034/0.034	13/13	0.050/0.050
$(\nu_4)^s$	1626.2803	1626.2744	80/80	0.006/0.006	21/21	0.004/0.004	24/24	0.006/0.006
$(\nu_4)^a$	1627.3867	1627.3724	80/80	0.011/0.011	21/21	0.012/0.012	25/25	0.017/0.017
$(3\nu_2)^s$	2384.1711		40/40	0.009/0.009	10/10	0.017/0.017	12/12	0.023/0.023
$(3\nu_2)^a$	2895.5336	2895.5218	40/40	0.015/0.015	11/11	0.040/0.040	13/13	0.054/0.054
$(\nu_2 + \nu_4)^s$	2540.4980	2540.5230	80/80	0.019/0.019	21/21	0.014/0.014		
$(\nu_2 + \nu_4)^a$	2586.1435	2586.1272	80/80	0.018/0.018	20/19	0.041/0.015		
$(2\nu_2 + \nu_4)^s$	3189.3784		9/0	0.659/	3/0	0.464/	1/0	1.170/
$(2\nu_2 + \nu_4)^a$	3502.5812		5/0	0.405/	2/0	0.347/	1/0	0.111/
$(2\nu_4^0)^s$	3215.9471		36/36	0.026/0.026	4/4	0.035/0.035	4/0	0.701/
$(2\nu_4^0)^a$	3217.5812	3217.5823	27/27	0.032/0.032	1/0	0.015/	2/0	0.770/
$(2\nu_4^2)^s$	3240.1535	3240.1623	74/72	0.044/0.039	14/11	0.086/0.062	1/0	0.534/
$(2\nu_4^2)^a$	3241.5812	3241.5965	71/69	0.031/0.031	8/7	0.079/0.073	2/0	0.207/
$(\nu_1)^s$	3336.1098		40/40	0.017/0.017	6/6	0.108/0.108		
$(\nu_1)^a$	3337.0801	3337.0971	40/40	0.008/0.008	6/5	0.039/0.031		
$(\nu_3)^s$	3443.6359	3443.6294	80/80	0.013/0.013	19/17	0.037/0.035		
$(\nu_3)^a$	3443.9984	3443.9878	80/80	0.014/0.014	18/16	0.032/0.032		
$(4\nu_2)^s$	3462.4101		12/0	0.099/	4/0	0.137/		
$(\nu_2 + 2\nu_4^0)^s$	4115.8584		3/0	0.062/				
$(\nu_2 + 2\nu_4^0)^a$	4173.0903		11/3	0.036/0.022	1/0	0.118/		
$(\nu_2 + 2\nu_4^2)^s$	4135.8304		24/18	0.094/0.095				
$(\nu_2 + 2\nu_4^2)^a$	4192.9435		20/11	0.049/0.035				
$(\nu_1 + \nu_2)^s$	4294.5397		40/40	0.035/0.035	6/1	0.101/0.043		
$(\nu_1 + \nu_2)^a$	4320.0052	4320.0306	40/40	0.047/0.047	10/8	0.114/0.113		
$(\nu_3 + \nu_2)^s$	4416.9586	4416.9151	76/64	0.028/0.027	1/0	0.029/	1/0	0.140/
$(\nu_3 + \nu_2)^a$	4435.4577	4435.4465	70/56	0.028/0.027	2/0	0.012/		
$(2\nu_2 + 2\nu_4^0)^a$	5093.5549		4/2	0.305/0.304				
$(2\nu_2 + 2\nu_4^2)^s$	4773.8184		1/0	0.022/				
$(2\nu_2 + 2\nu_4^2)^a$	5113.2536		1/1	1.585/1.585				
$(3\nu_4^1)^s(E)$	4799.2215		1/0	0.015/	1/0	0.213/		
$(3\nu_4^1)^a(E)$	4801.4128		1/0	0.038/				
$(3\nu_4^3)^s(A_2)$	4840.8899		1/0	0.087/				
$(\nu_1 + \nu_4)^s$	4955.7216	4955.7561	65/24	0.032/0.031	11/2	0.026/0.053	1/0	0.010/
$(\nu_1 + \nu_4)^a$	4956.8717		39/15	0.038/0.030	5/1	0.049/0.052	2/0	0.248/
$(\nu_1 + 2\nu_2)^s$	5000.2486		2/2	0.124/0.124				
$(\nu_3 + \nu_4)^s(A_2)$	5052.0195		5/3	0.032/0.017				
$(\nu_3 + \nu_4)^s(E)$	5052.6032		58/45	0.043/0.044	2/0	0.079/		
$(\nu_3 + \nu_4)^a(A_1)$	5052.6641		3/2	0.029/0.005				
$(\nu_3 + \nu_4)^a(E)$	5053.2343		26/16	0.063/0.048				
$(\nu_3 + \nu_4)^a(A_2)$	5067.7243		7/3	0.106/0.069				
$(\nu_3 + \nu_4)^s(A_1)$	5067.7812		12/8	0.057/0.061				
$(4\nu_2 + \nu_4)^s$	4530.6138		2/1	0.261/0.288				
$(4\nu_2 + \nu_4)^a$	5104.9370		1/1	0.017/0.017				
$(2\nu_2 + \nu_3)^s$	5144.9353		8/0	0.205/	2/0	0.462/		
$(2\nu_2 + \nu_3)^a$	5352.9840		12/0	0.117/				
$(\nu_1 + \nu_2 + \nu_4)^s$	5897.8022		1/0	0.004/				
$(\nu_1 + 2\nu_4^2)^s$			39/34	0.127/0.083				
$(\nu_1 + 2\nu_4^2)^a$			37/31	0.263/0.205				
$(\nu_1 + \nu_3)^s$			72/56	0.271/0.271				
$(\nu_1 + \nu_3)^a$			70/60	0.155/0.138				
$(2\nu_2 + 3\nu_4^1)^a$			2/2	1.820/1.820				
$(\nu_3 + 2\nu_4^2)^s$			64/46	0.144/0.095	1/0	0.190/		
$(\nu_3 + 2\nu_4^2)^a$			65/51	0.138/0.132	1/0	0.046/		
$(\nu_3 + 2\nu_4^0)^s$			5/4	0.072/0.065				
$(\nu_3 + 2\nu_4^0)^a$			5/3	0.259/0.184				
$(2\nu_3^0)^s$			26/19	0.152/0.097				
$(2\nu_3^0)^a$			28/23	0.257/0.174				
$(2\nu_3^2)^s$			16/13	0.047/0.052				
$(2\nu_3^2)^a$			16/11	0.084/0.096				

on BYTe and HSL-2, along with estimated band centers. Experimentally derived vibrational term values are provided for 9 out of the 14 symmetric and asymmetric bands present in MARVEL above 6300 cm^{-1}, with which our calculations typically agree to within 0.01-0.07 cm^{-1}.

Fig. 2 shows energy differences between MARVEL and NH3-C2018 above 6300 cm^{-1}. These show a slight deterioration in accuracy compared to our lower energy predictions, resulting in an increased σ_{rms} of roughly 0.1-0.2 cm^{-1} for states with $J = 0 - 8$. To provide a more reliable comparison, energies derived from only 1 or 2 transitions are not shown. Their associated rms deviations

Table 4
Vibrational band center labelling conflicts between different data sources for 6300–7000 cm^{-1} region.

Band #	Γ_{tot}	s/a	This work		HSL-pre3 [14,15]		MARVEL [6]	
1	E'	s	6556.3877	$\nu_1 + 2\nu_4^2$	6556.3990	$\nu_1 + 2\nu_4^2$	6556.4218	$\nu_1 + 2\nu_4^2$
	E''	a	6557.9091		6557.9065		6557.9306	
2	E'	s	6666.0662	$\nu_3 + 2\nu_4^2$	6666.1946	$\nu_3 + 2\nu_4^2$	–	
	E''	a	6665.7778		6665.7915		–	
3	E'	s	6608.7819	$\nu_1 + \nu_3$	6608.7773	$\nu_3 + 2\nu_4^0$	6608.8218	$\nu_1 + \nu_3$
	E''	a	6609.6907		6609.7031		6609.7532	
4	E'	s	6677.4899	$\nu_1 + \nu_3$	6677.4125	$\nu_1 + \nu_3$	6677.4317	$\nu_3 + 2\nu_4^2$
	E''	a	6678.1829		6678.1141		6678.3103	
5	A_2''	a	6795.2933	$2\nu_3^0$	6795.2529	$2\nu_3^0$	6795.3382	$2\nu_3^0$
	A_1'	s	6796.7741		6796.9054		–	
6	E'	s	6850.2303	$2\nu_3^2$	6850.1524	$2\nu_3^2$	6850.2449	$2\nu_3^2$
	E''	a	6850.6830		6850.5680		6850.6550	
7	E'	s	6314.0913	$2\nu_2 + 3\nu_4^1$	6313.1898	$2\nu_2 + 3\nu_4^1$	–	
	E''	a	6680.4035		6680.3736		–	

are, however, still included in Table 3, and show slightly worse agreement than those derived by 3 or more transitions, indicating that the experimental values may not all be correct. Several outliers that do not appear to conform to the general behaviour within their vibrational band are also noted, the most conspicuous of these MARVEL energies being 7355.7984, 7163.1765 and 7356.3801 cm^{-1}, with deviations of 1.959,-1.688 and 1.604 cm^{-1} respectively. Some may be explained by a difference in vibrational labelling, for example, the MARVEL state at 7355.7984 cm^{-1} is assigned to the $4\nu_2 + 2\nu_4^2$ band according to our labelling. So, too, are the MARVEL states at 6788.1366 and 6997.0047 cm^{-1} with residuals 1.215 and 0.777 cm^{-1}. Such large deviations would not be surprising considering no data from this band was sampled in the refinement. There are likely also to be issues with perturbations due to resonance interactions between vibrational states which have not been correctly represented in our PES; see the recent work on this by Mizus et al. [45].

Finally, we should mention that four MARVEL energies were not included in the above comparisons due to suspiciously large deviations from our calculations. The MARVEL state at 6788.1366 cm^{-1}, assigned to the $(\nu_3 + 2\nu_4^0)^a$ band, was removed from the rms statistics in Table 3 for reasons discussed above, but included in Fig. 2. States at 4446.5460, 5162.4116 and 5172.9416 cm^{-1}, derived from 3, 6 and 8 transitions respectively, were also removed from all comparisons due to large residuals which we cannot explain.

3.3. Intensity simulations

To simulate absolute absorption intensities we use the expression [46] as implemented in the EXOCROSS program [47]

$$I(f \leftarrow i) = \frac{8\pi^3 N_A \nu_{if} \exp(-E''/kT)[1 - \exp(-hc\nu_{if}/kT)]}{(4\pi\epsilon_0)3hcQ}$$
$$\times \sum_{\Phi_{int}' \Phi_{int}''} \sum_{A=X,Y,Z} |\langle \Phi_{int}' | \mu_A | \Phi_{int}'' \rangle|^2,$$

where Φ_{int}' and Φ_{int}'' are the upper and lower state wavefunctions respectively, that correspond to energies E' and E''. ν_{if} is the transition wavenumber, T is the temperature, $Q(T)$ is the total internal partition function and μ_A is the electronically averaged component of the molecular dipole moment along the $A = X, Y, Z$ axis. The two requirements, therefore, for accurate line intensities are high quality wavefunctions and a high quality DMS.

Our intensity calculations employ the well-established dipole moment surface (DMS) of Yurchenko et al. [48] (denoted DMS-B), which was used in the construction of the BYTe line list. We also use this opportunity to report preliminary results for a new surface currently under construction (denoted DMS-1). For this DMS, dipole moment components μ_A were calculated using the finite

field procedure with an external field value of $\pm 5 \times 10^{-5}$ a.u. For both water [49] and carbon dioxide [50] we have demonstrated that even though the finite field method requires seven times more computations than using expectation values, the resulting DMS is more accurate. Calculations were performed using internally contracted MRCI in the full valence reference space comprising 8 electrons in 7 orbitals, with the aug-cc-pwCVQZ basis set. The same grid of 50 000 nuclear geometries used by Polyansky et al. [17] was employed, although only 10 782 points were computed successfully. The final fit included 9498 points that were reproduced with an unweighted rms error of 0.0009 D. The Molpro 2012 package [51] was used for all calculations.

Line list calculations were performed at room temperature (296 K) using a partition function value of $Q(T) = 1725.224746$ [52]. Transitions cover states with $J = 0 - 20$ within the frequency range $0 - 20\,000$ using DMS-B or $0 - 12\,000$ cm^{-1} using DMS-1. No intensity cut-off was used for either line list. Einstein-A coefficients were calculated using the program GAIN [53] which was developed as part of TROVE [29]. Our two line lists are provided in the ExoMol [54] format are available from the ExoMol website (www.exomol.com); details of NH$_3$ specific formatting are the same as for BYTe [11].

Fig. 3 displays the ratio of our predicted line intensities (DMS-B) to the experimental values ($I_{obs} > 1 \times 10^{-24}$ cm^{-1}/(molecule cm^{-2})) taken from HITRAN2016 for the 0–7000 cm^{-1} region. Only results for DMS-B are shown, however, DMS-1 performed similarly. The majority of lines fall within $\pm 20\%$ of experiment. The experimental uncertainty [4] varies substantially between different sources and we do not consider it here. Coloured in Fig. 3 are strong bands in the 6300–7000 cm^{-1} region, for which over 4000 lines in HITRAN are unassigned. Corresponding I_{calc}/I_{obs} numerical values for the strongest lines assigned to each band are given in Table 5.

We note that the $5700 - 6200$ cm^{-1} region is completely missing from HITRAN. In this region we predict strong absorption by the $\nu_2 + \nu_3 + \nu_4$ band (calculated band center $s/a = 6012.8563/6036.5254$ cm^{-1}, calculated DMS-B band intensity $s/a = 4.841/4.840 \times 10^{-20}$ cm/molecule), the $\nu_1 + \nu_2 + \nu_4$ band ($s/a = 5897.8022/5930.8407$ cm^{-1}, $1.929/3.362 \times 10^{-21}$ cm/molecule) and the $(3\nu_2 + \nu_3)^s$ band (5856.0580 cm^{-1}, 5.752×10^{-21} cm/molecule). These intensity values are in good agreement between both DMSs, and those given in BYTe [11].

Recently Vander Auwera and Vanfleteren [55] measured line intensities of the 7400–8600 cm^{-1} region with an estimated accuracy of 10% for most strong lines. Their measurements validated Barton et al.'s [21,22] estimated uncertainty of 15% for lines weaker than 1×10^{-22} cm^{-1}/(molecule cm^{-2}), but suggested that their uncertainty is significantly more for stronger lines. Our synthetic spectra,
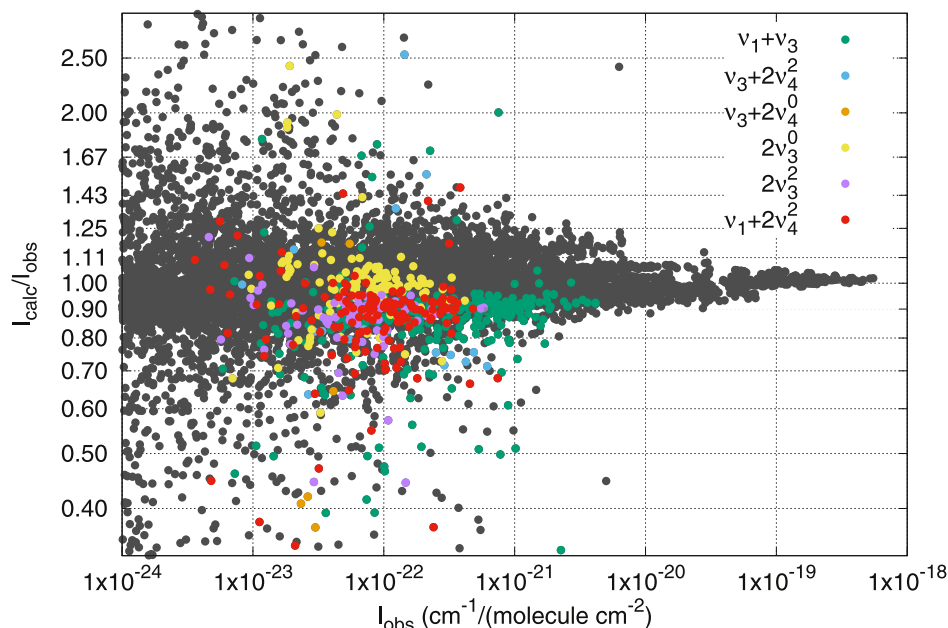
Fig. 3. Ratio of calculated to observed line intensities for lines taken from 0– to 7000 cm^{-1} region of HITRAN2016. Coloured are transitions assigned to strong bands in the 6300–7000 cm^{-1} region. Vibrational labels are taken from HITRAN2016.
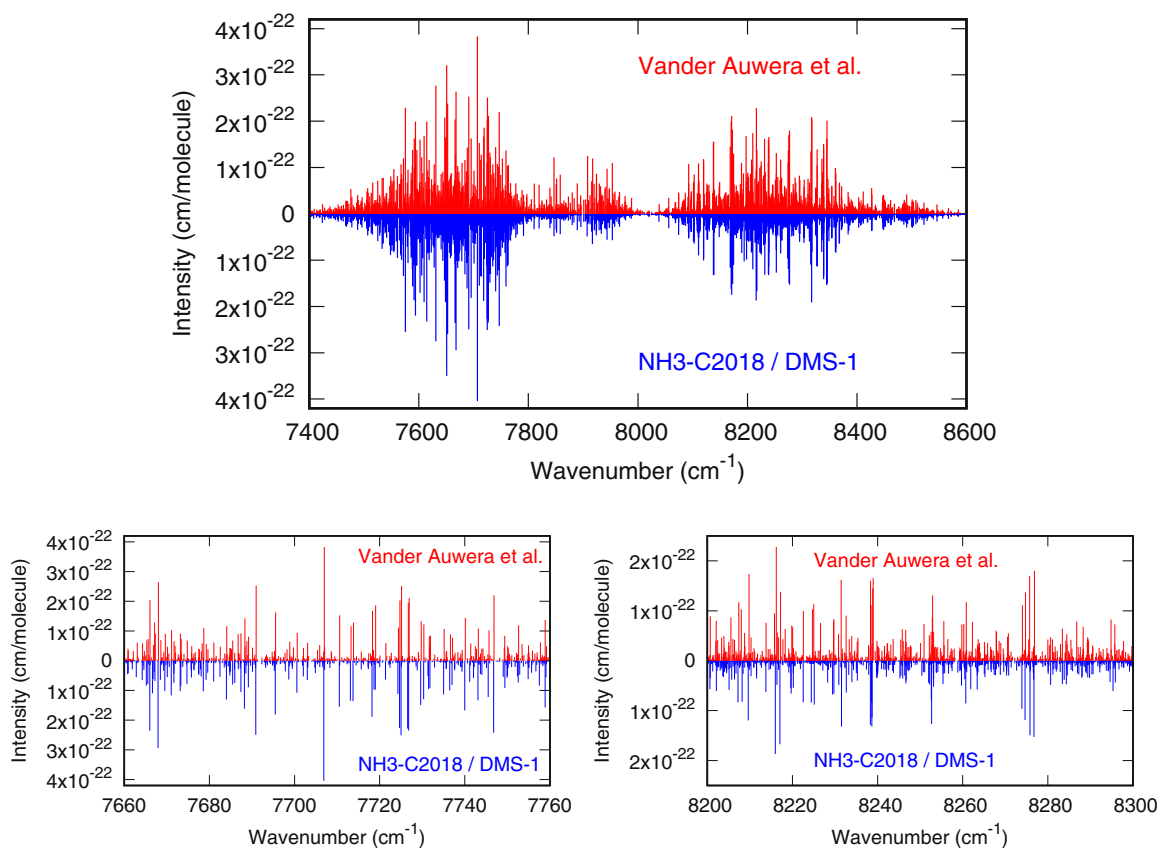

Fig. 4. Comparison of the simulated (TROVE) and observed [55] spectra of NH$_3$ at $T = 293$ K for 7400–8600 cm^{-1} region, with expansions of the 7660–7750 cm^{-1} region (bottom left) and 8160–8240 cm^{-1} region (bottom right).

calculated using DMS-1 and DMS-B, is temperature adjusted and compared with their works in Figs. 4 and 5. Numerical comparisons between our calculated intensities and those of Vander Auwera and Vanfleteren [55], for the strongest lines included in our assignments (detailed in Section 3.4), are also provided in Table 5.

From Figs. 4 and 5 we see that qualitative agreement is good and the dominant spectral features are reproduced well by our calculations, although there is a notable reduction in line position accuracy beyond 8000 cm^{-1} that could undoubtedly be improved with the availability of additional high energy assignments. Of the bands covered by our assignments, DMS-1 reproduces intensities

Table 5

Comparison of calculated intensities to the experimentally derived values taken from HITRAN2016 [4] below 7000 cm^{-1} and Vander Auwera and Vanfleteren [55] above 7000 cm^{-1}. Line positions are given in cm^{-1}, energies in cm^{-1} and intensities in cm^{-1}/(molecule cm^{-2}). Quantum labels below 7000 cm^{-1} are taken from HITRAN2016; assignments above 7000 cm^{-1} are those of this work, detailed in Section 3.4.

ν_{obs}	obs-calc	$(J'K'L_3L_4i')$	$(J''K''i'')$	Band	Intensity	I$_{DMS-1}$/I$_{obs}$	I$_{DMS-B}$/I$_{obs}$
6678.5355	0.0173	(5,4,1,0,s)	(4,3,s)	$\nu_1 + \nu_3$	2.94×10^{-21}	0.918	0.924
6678.3094	0.0715	(5,4,1,0,a)	(4,3,a)	$\nu_1 + \nu_3$	2.95×10^{-21}	0.914	0.921
6605.1042	0.0733	(2,1,1,0,a)	(2,0,a)	$\nu_1 + \nu_3$	3.31×10^{-21}	0.923	0.935
6605.6088	0.0485	(3,1,1,0,s)	(3,0,s)	$\nu_1 + \nu_3$	3.61×10^{-21}	0.916	0.924
6658.9067	0.0237	(4,4,1,0,s)	(3,3,s)	$\nu_1 + \nu_3$	4.15×10^{-21}	0.913	0.924
6658.9585	0.0543	(4,4,1,0,a)	(3,3,a)	$\nu_1 + \nu_3$	4.15×10^{-21}	0.907	0.921
6594.6488	−0.1022	(6,2,0,2,a)	(6,3,a)	$\nu_1 + 2\nu_4$	3.03×10^{-22}	0.866	0.850
6516.9777	0.0625	(3,3,0,2,a)	(4,4,a)	$\nu_1 + 2\nu_4$	3.15×10^{-22}	1.193	1.176
6588.6147	−0.0082	(4,2,0,2,a)	(4,3,a)	$\nu_1 + 2\nu_4$	3.22×10^{-22}	0.918	0.903
6593.1306	0.0462	(5,2,0,2,s)	(5,3,s)	$\nu_1 + 2\nu_4$	3.25×10^{-22}	0.950	0.936
6516.5066	0.0470	(3,3,0,2,s)	(4,4,s)	$\nu_1 + 2\nu_4$	3.28×10^{-22}	0.983	0.975
6588.8617	−0.0346	(4,4,0,2,a)	(3,3,a)	$\nu_1 + 2\nu_4$	3.28×10^{-22}	0.805	0.815
6660.1180	0.0605	(2,2,1,2,s)	(2,1,s)	$\nu_3 + 2\nu_4$	2.50×10^{-22}	0.914	0.755
6608.7807	0.0557	(2,1,1,2,s)	(3,0,s)	$\nu_3 + 2\nu_4$	2.90×10^{-22}	0.892	0.716
6660.6045	0.0392	(3,2,1,2,s)	(3,1,s)	$\nu_3 + 2\nu_4$	3.24×10^{-22}	0.911	0.747
6720.2025	0.0391	(3,2,1,2,s)	(2,1,s)	$\nu_3 + 2\nu_4$	4.24×10^{-22}	0.872	0.727
6625.5751	0.1011	(3,3,1,2,s)	(4,4,s)	$\nu_3 + 2\nu_4$	4.88×10^{-22}	0.860	0.755
6708.1286	0.0552	(2,1,1,2,s)	(1,0,s)	$\nu_3 + 2\nu_4$	6.17×10^{-22}	0.897	0.713
6806.1019	−0.0125	(2,2,2,0,a)	(3,3,a)	$2\nu_3$	2.33×10^{-22}	0.644	0.896
6806.4960	0.0088	(2,2,2,0,s)	(3,3,s)	$2\nu_3$	2.40×10^{-22}	0.619	0.881
6919.3989	0.0625	(5,5,2,0,a)	(4,4,a)	$2\nu_3$	3.04×10^{-22}	0.725	0.901
6919.8462	0.0533	(5,5,2,0,s)	(4,4,s)	$2\nu_3$	3.15×10^{-22}	0.691	0.901
6906.1648	0.0594	(4,4,2,0,a)	(3,3,a)	$2\nu_3$	5.53×10^{-22}	0.720	0.902
6906.6178	0.0434	(4,4,2,0,s)	(3,3,s)	$2\nu_3$	5.81×10^{-22}	0.688	0.906
6733.7655	0.0344	(2,0,0,0,a)	(3,0,s)	$2\nu_3$	2.25×10^{-22}	0.961	0.998
6794.3775	0.0373	(4,4,0,0,a)	(4,4,s)	$2\nu_3$	2.78×10^{-22}	0.702	0.728
6794.3252	0.0938	(6,6,0,0,s)	(6,6,a)	$2\nu_3$	2.82×10^{-22}	0.919	0.977
6794.1728	0.0501	(6,6,0,0,a)	(6,6,s)	$2\nu_3$	3.12×10^{-22}	0.897	0.932
6794.9559	0.1193	(3,3,0,0,s)	(3,3,a)	$2\nu_3$	3.30×10^{-22}	0.958	1.023
6794.5460	0.0398	(3,3,0,0,a)	(3,3,s)	$2\nu_3$	4.15×10^{-22}	0.898	0.932
6670.3905	0.0230	(1,0,1,0,s)	(1,1,s)	$\nu_3 + 2\nu_4$	3.00×10^{-23}	0.633	0.370
6733.5643	0.1246	(6,1,1,0,s)	(5,2,s)	$\nu_3 + 2\nu_4$	3.34×10^{-23}	1.188	1.180
6610.1639	−0.1529	(2,0,1,0,a)	(3,1,a)	$\nu_3 + 2\nu_4$	4.11×10^{-23}	0.877	0.645
6476.6566	0.1243	(6,1,1,0,s)	(7,2,s)	$\nu_3 + 2\nu_4$	5.49×10^{-23}	1.197	1.174
6709.4788	−0.1533	(2,0,1,0,a)	(1,1,a)	$\nu_3 + 2\nu_4$	9.76×10^{-23}	0.950	0.802
6614.8541	0.1251	(6,1,1,0,s)	(6,2,s)	$\nu_3 + 2\nu_4$	1.78×10^{-23}	0.920	0.908
7614.6136	0.0202	(2,2,1,0,s)	(3,3,s)	$\nu_1 + \nu_2 + \nu_3$	1.99×10^{-22}	1.172	0.803
7631.1622	0.0443	(2,2,1,0,a)	(3,3,a)	$\nu_1 + \nu_2 + \nu_3$	2.77×10^{-22}	0.998	0.653
7726.9126	0.0999	(4,1,1,0,s)	(3,0,s)	$\nu_1 + \nu_2 + \nu_3$	2.11×10^{-22}	1.119	0.743
7725.1459	0.1097	(5,4,1,0,s)	(4,3,s)	$\nu_1 + \nu_2 + \nu_3$	2.51×10^{-22}	1.003	0.683
7746.8743	0.1148	(7,7,1,0,a)	(6,6,a)	$\nu_1 + \nu_2 + \nu_3$	2.20×10^{-22}	1.103	0.669
7650.9806	0.0972	(3,1,1,0,s)	(3,0,s)	$\nu_1 + \nu_2 + \nu_3$	3.21×10^{-22}	1.096	0.743
7616.1245	0.0087	(2,1,1,2,a)	(3,3,s)	$\nu_2 + \nu_3 + 2\nu_4$	9.37×10^{-23}	0.912	0.611
7640.9146	0.1433	(5,4,1,0,s)	(4,3,s)	$\nu_2 + \nu_3 + 2\nu_4$	8.62×10^{-23}	0.891	0.853
7651.8952	0.0597	(3,1,1,0,a)	(2,0,a)	$\nu_2 + \nu_3 + 2\nu_4$	8.49×10^{-23}	0.912	0.757
7618.7724	0.0758	(4,4,1,0,s)	(3,3,s)	$\nu_2 + \nu_3 + 2\nu_4$	1.16×10^{-22}	0.861	0.835
7678.6769	0.1163	(7,7,1,0,a)	(6,6,a)	$\nu_2 + \nu_3 + 2\nu_4$	1.10×10^{-22}	0.935	0.879
7724.4123	0.1198	(5,5,1,2,a)	(4,4,a)	$\nu_2 + \nu_3 + 2\nu_4$	1.11×10^{-22}	1.009	0.568
7924.2364	0.1965	(5,4,2,0,s)	(4,3,s)	$\nu_2 + 2\nu_3$	8.65×10^{-23}	0.541	0.875
7943.7660	0.0986	(7,7,2,0,s)	(6,6,s)	$\nu_2 + 2\nu_3$	9.77×10^{-23}	0.573	0.922
7953.4006	0.0143	(7,7,2,0,a)	(6,6,a)	$\nu_2 + 2\nu_3$	1.10×10^{-22}	0.519	0.830
7917.1851	0.0816	(4,4,2,0,a)	(3,3,a)	$\nu_2 + 2\nu_3$	1.19×10^{-22}	0.551	0.886
7908.1402	0.6560	(4,4,2,0,s)	(3,3,s)	$\nu_2 + 2\nu_3$	1.25×10^{-22}	0.390	0.615
7846.8068	0.0816	(3,1,2,0,s)	(3,0,s)	$\nu_2 + 2\nu_3$	1.22×10^{-22}	0.397	0.665

of the $\nu_1 + \nu_2 + \nu_3$ and $\nu_2 + \nu_3 + 2\nu_4$ bands excellently, often to within 10% of the experimental value, but severely underestimates the $\nu_2 + 2\nu_3^2$ band (see Table 5). In contrast, DMS-B reproduces the $\nu_2 + 2\nu_3^2$ band somewhat better, but consistently underestimates the $\nu_1 + \nu_2 + \nu_3$ and $\nu_2 + \nu_3 + 2\nu_4$ bands. For this reason we chose to use DMS-1 for our assignments in Section 3.4. We suspect that by employing a denser, more extensive grid of geometries in our fit, the underestimated intensities of DMS-1 will be resolved. This work is currently in progress, and we expect a refitted dipole moment surface to become available in the near future. However, in order to extend a similarly high level of accuracy above 8000 cm^{-1}, higher quality wavefunctions will also be required.

Beyond 10 400 cm^{-1} estimating the reliability of our line lists is difficult owing to the lack of data between the regions studied by Barton et al. [22] and Zobov et al. [23]. Errors on line positions may be tens of wavenumbers for bending and combination bands due to basis set convergence errors and lack of constraint during the refinement. For these reasons we do not advocate relying on our line list to guide high resolution spectroscopic studies above 12 000 cm^{-1} except for the $5\nu_{NH}$ and $6\nu_{NH}$ bands with low bending excitation. Our final recommendation for general use is DMS-B, or DMS-1 below 7800 cm^{-1}.

3.4. Assignment of the 7400–8000 cm^{-1} region

Our fits raised a number of issues with the assignments of Barton et al. [21] and our improved potential should facilitate line assignments in the near-infrared region. We therefore undertook a
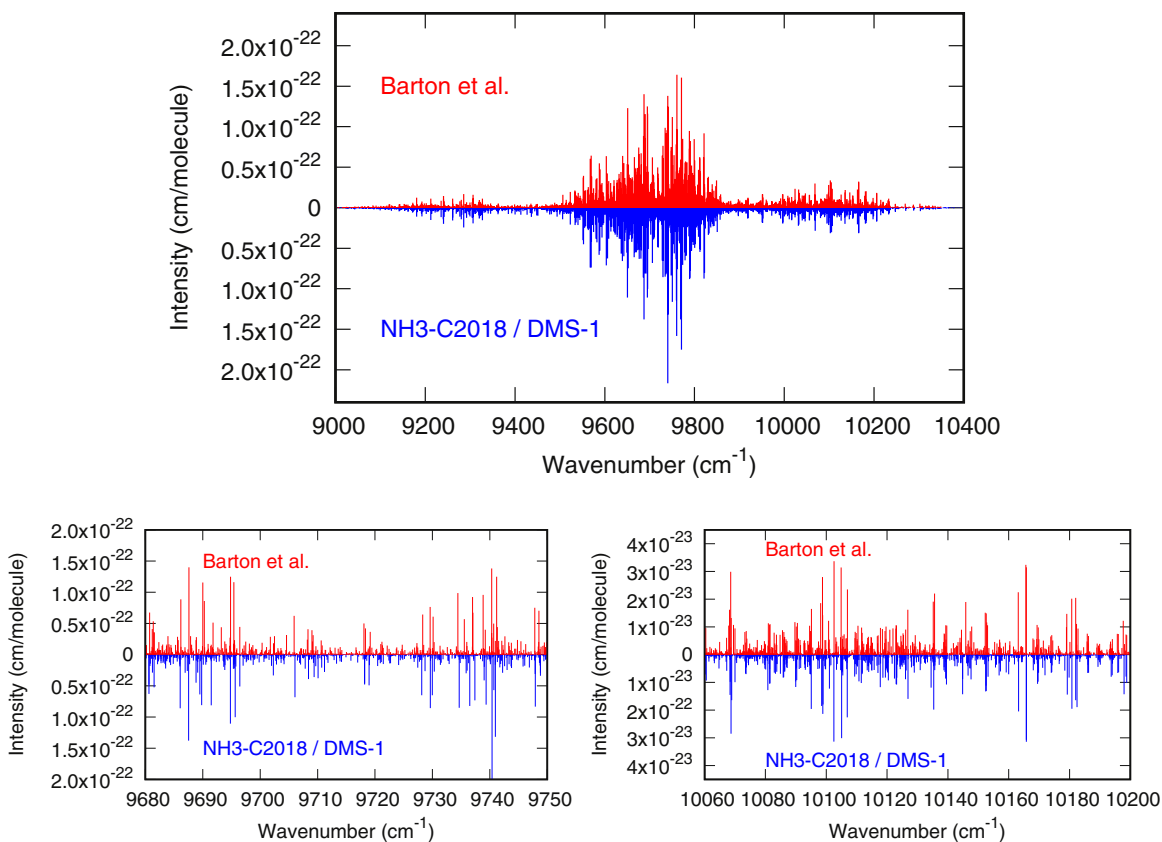
Fig. 5. Comparison of the simulated (TROVE) and observed [5] spectra of NH_3 at $T = 296$ K for 9000–10400 cm^{-1} region, with expansions of the 9680–9750 cm^{-1} region (bottom left) and 10060–10140 cm^{-1} region (bottom right).

re-analysis of the observed spectrum in the 7400–8000 cm^{-1} region. 769 lines from the 7400–8000 cm^{-1} region of the Barton et al. line list [21] were assigned using ground state combination differences (GSCDs). The method involves first performing tentative assignments based on a visual comparison between experimental and theoretical line lists. Theoretical upper state energies of each assignment are then replaced with empirical values calculated by adding the MARVEL lower state energies to the observed line positions. A tentative assignment is then considered validated if one or more additional unblended transitions sharing the same upper state (as the tentative assignment) can then be identified in both theoretical and experimental line lists to within the measurement uncertainty.

Our tolerance for accepting GSCD partners was ± 0.003 cm^{-1}, which was the same as used by Barton et al. [21] for their unblended assignments in this region. For line intensities, the ratio I_{obs}/I_{calc} for the GSCD partners were required to fall within 2/3 and 3/2 times the ratio of I_{obs}/I_{calc} for the manual assignment. This accounted for the variation in accuracy between different vibrational bands, in particular the underestimated $\nu_2 + 2\nu_3^2$ band discussed in Section 3.3. Tentative assignments were performed using the online assignment tool Spectropedia [56]. As a measure of confidence, each tentative assignment was placed into one of three categories based on its judged reliability. For the least reliable assignments (Flag C in Table 7), three additional GSCD partners were required for it to be considered validated. More reliable tentative assignments required either one or two additional GSCD partners (Flags A and B in Table 7), one being reserved only for strong, isolated lines. After applying these validation criteria only 284 of our 827 initial hand assignments were accepted into the final list. GSCD partners could be found for more transitions but these did not fulfil our minimum requirements to be retained.

Even despite stringent measures, the possibility of false partners must be considered. For weak lines with intensity $I < 5.0 \times 10^{-24}$ $cm^{-1}/(molecule$ $cm^{-2})$, there is an average of 0.022 lines per 0.006 cm^{-1} interval. Assuming a Poisson distribution, this translates to roughly a 1 in 47 chance of such a match being false. This probability reduces significantly for medium and strong lines ($I > 5.0 \times 10^{-24}$ $cm^{-1}/(molecule$ $cm^{-2})$) that contribute $\sim 2/3$ of our overall GSCD partners. For our assignments the overall standard deviation of our derived upper state energies is 0.0009 cm^{-1}, and only in a few cases does the range of derived upper state energies within a GSCD set exceed 0.003 cm^{-1}. This, combined with the additional assurances provided by intensity comparisons, practically eliminates the possibility of fortuitous matches.

A summary of our final list of assignments is presented in Table 6. The empirical upper state energy of each GSCD set was calculated by averaging the observed line positions plus the MARVEL lower state energies. In total we assigned rovibrational quanta for 769 transitions and upper state energies for 284 levels, spanning an estimated 11 vibrational bands. Vibrational labels are taken from the leading coefficient basis set contributor in our variational calculation, which were as low as 0.22 for some bands listed in Table 6, and indeed (0.08) lower for the $2\nu_1 + \nu_2$ band which was highly mixed. Rotationally excited states may also possess significantly smaller leading coefficients. Thus, all vibrational labelling should be viewed as tentative. Fig. 7 compares the energies calculated using our new PES to those empirically derived from our assignments. Residuals are seen to have a systematic dependence on rotational quanta, although this is partly obscured by mixing between states in the $\nu_1 + \nu_2 + \nu_3^1$ and $\nu_1 + \nu_2 + 2\nu_4^0$ bands, possibly due to our heavy reliance on these bands during the refinement. This systematic behaviour, apart from highlighting deficien-
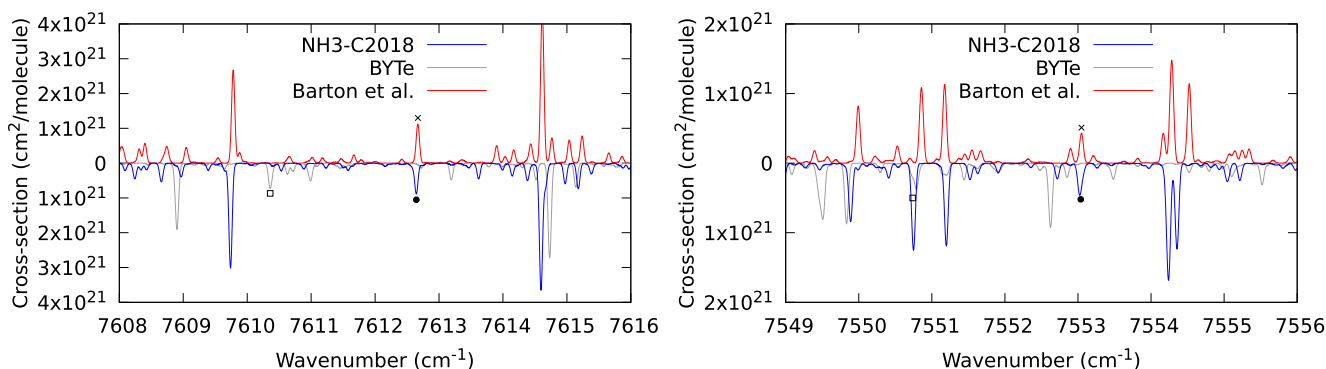
Fig. 6. Sample combination difference pair that were reassigned during our analysis. Lines convoluted with a gaussian profile HWHM=0.06.

Table 6

An overview of the assignments from this work. Only the E-symmetry band origin for the $\nu_2 + \nu_3 + 2\nu_4^2$ band is shown, although our assignments include A_1 and A_2-symmetry vibrational states as well.

Band	s/a	Center (cm^{-1}) (This work)		N_{lines}	N_{eners}
$\nu_1 + \nu_2 + \nu_3^1$	s	7656.6402		160	56
	a	7673.4138		137	50
$\nu_2 + \nu_3 + 2\nu_4^0$	s	7567.8000		90	31
	a	7597.5458		98	36
$\nu_2 + \nu_3 + 2\nu_4^2$	s	7605.9881	(E)	35	11
	a	7640.2230	(E)	28	11
$\nu_1 + \nu_2 + 2\nu_4^2$	s	7484.6131		9	4
	a	7525.9480		12	6
$\nu_2 + 2\nu_3^2$	s	7854.3016		99	39
	a	7864.1066		98	40
$2\nu_1 + \nu_2$	s	7575.3439		3	1

cies in the NH3-C2018 PES, further reassures us of the reliability of our assignments.

There is significant overlap between our work and that of Barton et al. [21] who previously assigned 230 of the lines in our current analysis. 177 of these, all assigned by combination difference (CD) bar one, agree with our assignments in at least J and total symmetry, and so we consider these assignments validated. The 53 that disagree consist of 9 unblended CD lines, 17 blended CD lines, and 27 assigned using the method of branches [24]. The method of branches allows for small systematic differences between theory and experiment within a vibrational band with increasing J. However, it fails if this dependency is large and there are gaps in experimental values which act as predictors. Therefore occasional misassignments are not surprising. For the 9 disagreeing CD states, 7 were previously assigned to the $\nu_1 + \nu_2 + 2\nu_4^2$ band for which BYTe reproduces the Kitt Peak spectral features particularly poorly. Fig. 6 shows absorption cross-sections of a sample CD pair that were reassigned during our analysis, in this case the experimental line at 7612.6690 cm^{-1} (cross) was reassigned from $E''(3,3)^s \leftarrow E'(2,2)^s$ (hollow square) to $A_2'(1,1)^a \leftarrow A_2''(0,0)^a$ (filled circle), and its partner line at 7553.0483 (cross) was reassigned from $E''(3,3)^s \leftarrow E'(3,2)^s$ (hollow square) to $A_2'(1,1)^a \leftarrow A_2''(2,0)^a$ (filled circle). Here, our notation corresponds to $\Gamma_{tot}(J, K)^{s/a}$. For the purposes of Fig. 6 lines are convoluted with a Gaussian profile, HWHM=0.06 cm^{-1}. A complete list of conflicts and agreements is included with our list of assignments in the supplementary material. Whilst our assignments account for only 47.5% of the summed intensity for this region, our aim was not complete assignment. Rather, to demonstrate the predictive power of our line list in this newly charted region, and extract a reliable list of energies that can be used to refine future *ab initio* calculations. We expect our line list to also be useful for assignments up to 10 400 cm^{-1}, although we have made no attempt to do so here.

Table 7

Examples of the GSCD process for 6 different derived upper states. Units of energy and frequency are cm^{-1}, units of intensity are cm^{-1}/(molecule cm^{-2}). $\langle E'_{obs} \rangle$ is the averaged experimental energy.

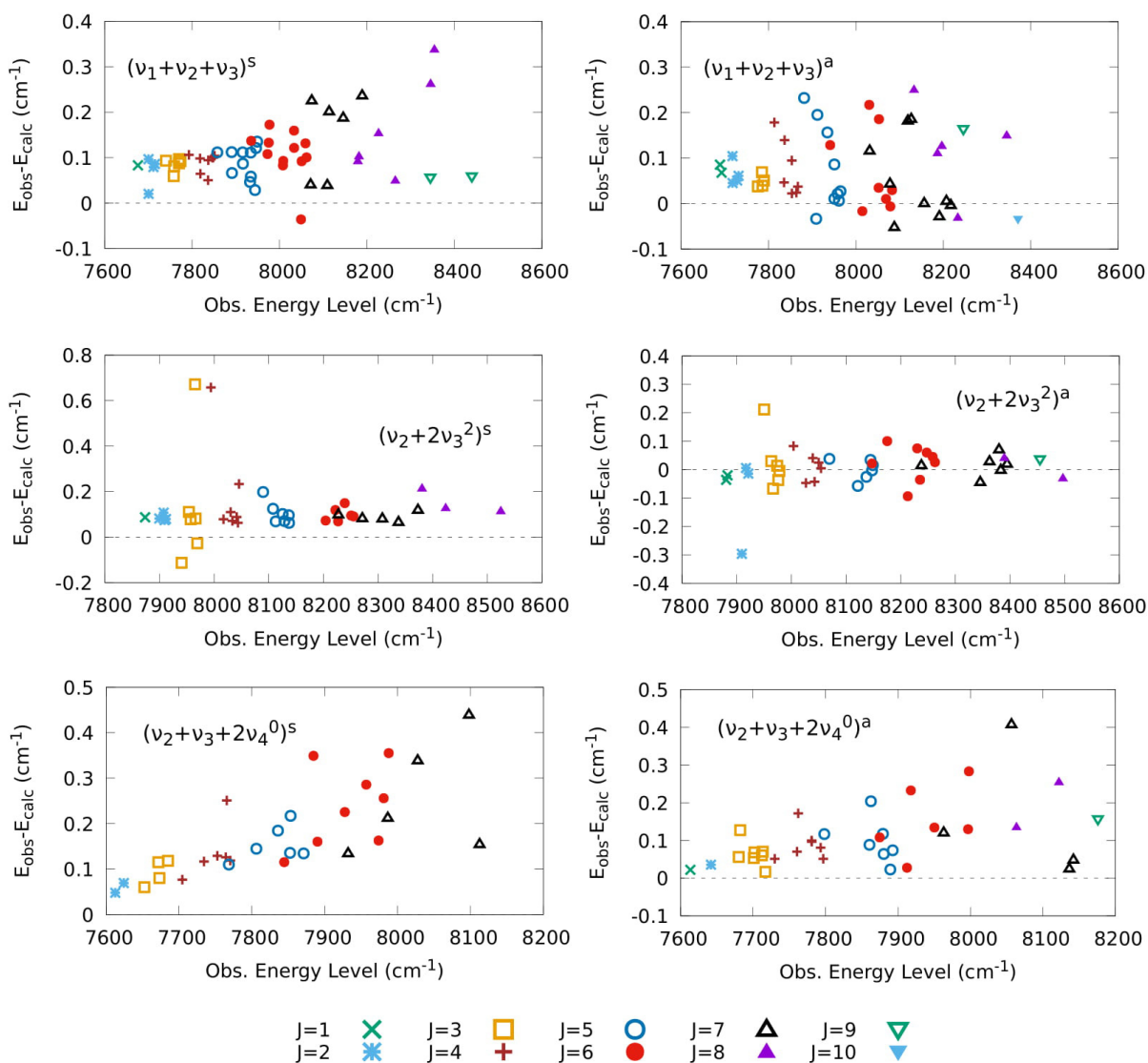| Flag	$(J'K'i')$	$(J''K''i'')$	Band	ν_{obs}	ν_{o-c}	E'_{obs}	E'_{calc}	$\langle E'_{obs} \rangle$	I_{obs}	I_{obs}/I_{calc}
A	(2, 1, a)	(3, 2, a)	$\nu_1 + \nu_2 + \nu_3$	7622.9614	0.0503	7728.1451	7728.0948	7728.1452	8.150×10^{-23}	0.970
A	(2, 1, a)	(2, 2, a)	$\nu_1 + \nu_2 + \nu_3$	7682.5580	0.0505	7728.1453	7728.0948	7728.1452	4.911×10^{-23}	0.905
B	(3, 2, a)	(4, 1, a)	$\nu_1 + 2\nu_2 + 2\nu_4^0$	7506.2948	0.0673	7701.9061	7701.8388	7701.9061	8.359×10^{-24}	1.094
B	(3, 2, a)	(3, 1, a)	$\nu_1 + 2\nu_2 + 2\nu_4^0$	7585.6281	0.0675	7701.9063	7701.8388	7701.9061	2.334×10^{-23}	0.989
B	(3, 2, a)	(2, 1, a)	$\nu_1 + 2\nu_2 + 2\nu_4^0$	7645.1972	0.0676	7701.9064	7701.8388	7701.9061	4.199×10^{-23}	1.096
C	(6, 1, a)	(5, 1, a)	$\nu_1 + 2\nu_2 + 2\nu_4^0$	7757.0252	0.1115	8050.9935	8050.8820	8050.9935	1.440×10^{-23}	1.012
C	(6, 1, a)	(7, 1, s)	$\nu_1 + 2\nu_2 + 2\nu_4^0$	7500.2346	0.1112	8050.9932	8050.8820	8050.9935	3.149×10^{-23}	1.223
C	(6, 1, a)	(6, 1, s)	$\nu_1 + 2\nu_2 + 2\nu_4^0$	7638.3694	0.1117	8050.9937	8050.8820	8050.9935	1.842×10^{-24}	0.834
C	(6, 1, a)	(5, 2, a)	$\nu_1 + 2\nu_2 + 2\nu_4^0$	7767.3768	0.1114	8050.9934	8050.8820	8050.9935	9.473×10^{-24}	0.916
A	(1, 0, s)	(2, 1, s)	$\nu_1 + \nu_2 + \nu_3$	7620.2164	0.0830	7676.1551	7676.0721	7676.1550	5.574×10^{-23}	0.883
A	(1, 0, s)	(1, 1, s)	$\nu_1 + \nu_2 + \nu_3$	7659.9820	0.0829	7676.1550	7676.0721	7676.1550	6.581×10^{-23}	0.946
B	(7, 2, s)	(8, 3, s)	$\nu_2 + 2\nu_3^2$	7693.5363	0.1174	8372.8243	8372.7069	8372.8252	4.247×10^{-24}	2.133
B	(7, 2, s)	(7, 3, s)	$\nu_2 + 2\nu_3^2$	7851.2037	0.1188	8372.8257	8372.7069	8372.8252	8.787×10^{-24}	1.713
B	(7, 2, s)	(6, 3, s)	$\nu_2 + 2\nu_3^2$	7989.5070	0.1186	8372.8255	8372.7069	8372.8252	6.677×10^{-24}	2.026
C	(6, 2, s)	(7, 1, s)	$\nu_1 + \nu_2 + \nu_3$	7498.2354	−0.0374	8048.9940	8049.0314	8048.9936	3.656×10^{-24}	0.825
C	(6, 2, s)	(7, 4, a)	$\nu_1 + \nu_2 + \nu_3$	7552.3180	−0.0374	8048.9940	8049.0314	8048.9936	3.855×10^{-24}	1.050
C	(6, 2, s)	(6, 1, s)	$\nu_1 + \nu_2 + \nu_3$	7636.3684	−0.0387	8048.9927	8049.0314	8048.9936	1.187×10^{-23}	0.919
C	(6, 2, s)	(5, 1, s)	$\nu_1 + \nu_2 + \nu_3$	7755.0233	−0.0398	8048.9916	8049.0314	8048.9936	2.974×10^{-23}	1.208
C	(6, 2, s)	(5, 2, a)	$\nu_1 + \nu_2 + \nu_3$	7765.3791	−0.0357	8048.9957	8049.0314	8048.9936	1.015×10^{-24}	1.122

Fig. 7. Agreement between energy levels derived from our assignments and the values predicted using NH3-C2018 for 6 vibrational bands.

4. Conclusion

We present an improved potential energy surface for $^{14}NH_3$, produced by empirical refinement of a high accuracy *ab initio* PES [17] to experimentally derived energy levels [21,35], and a number of our own assignments. The resulting rovibrational energy levels reproduce the MARVEL experimentally derived values for states with $J = 0 - 10$ with an rms deviation of 0.10 cm^{-1} under 6400 cm^{-1}, and 0.28 cm^{-1} between 6400 and 7555 cm^{-1}, although the reliability of some higher energy MARVEL states is uncertain.

Using a well established DMS [48], a new DMS currently under construction, and our own NH3-C2018 potential energy surface, room temperature line list calculations were performed for transitions between states with $J = 0 - 20$, in the frequency ranges 0–20 000 cm^{-1}, and 0–12 000 cm^{-1} respectively. Several strong bands in the 5700–6200 cm^{-1} were noted missing from HITRAN2016.

Our line lists were used to assign 769 transitions in the 7400–8000 cm^{-1} frequency range using ground state combination differences, and derive 284 upper state energies. Of our assignments, 230 lines were previously assigned [21], out of which we found 53 disagreed in at least one 'good' quantum number. Our use of stricter validation criteria and higher accuracy line lists suggests

that a handful of the previous assignments were incorrect. We hope that future analysis above 8000 cm^{-1} can validate the current assignments, and in turn inform future *ab initio* calculations. In this context we note the recent use of our NH$_3$ line list by Irwin et al. [57] to study ammonia spectra in Jupiter at near-infrared and visible wavelengths. Their comparisons suggest that the line list represents a significant improvement on what is currently available but that further work is need to improve the predicted frequencies at shorter wavelengths.

Our next aim is to use our PES in conjunction with DMS-B [48] to compute a hot line list for the frequency range 0–12 000 cm^{-1} suitable for use up to 1500 K. In order to achieve greater than 99% convergence of the partition function, our lower state energy threshold will necessarily be extended to 11 000 cm^{-1}, and our rotational excitations to at least $J = 42$. The resulting line list is to be included in the ExoMol database [54].

Supplementary material

Supplementary material associated with this article can be found, in the online version, at doi:10.1016/j.jqsrt.2018.07.022.

References

[1] Csaszar AG, Furtenbacher T. Promoting and inhibiting tunneling via nuclear motions. Phys Chem Chem Phys 2016;18:1092–104. doi:10.1039/c5cp04270d.

[2] Galloway JN, Aber JD, Erisman JW, Seitzinger SP, Howarth RW, Cowling EB, Cosby BJ. The nitrogen cascade. Bioscience 2003;53:341–56. doi:10.1641/0006-3568(2003)053[0341:TNC]2.0.CO;2.

[3] Erisman J.W., Galloway J.N., Seitzinger S., Bleeker A., Dise N.B., Petrescu A.M.R., Leach A.M., de Vries W.. Consequences of human modification of the global nitrogen cycle. Phil. Trans. Royal Soc. London B 368. doi:10.1098/rstb.2013.0116

[4] Gordon IE, Rothman LS, Hill C, Kochanov RV, Tan Y, Bernath PF, Birk M, Boudon V, Campargue A, Chance KV, Drouin BJ, Flaud JM, Gamache RR, Hodges JT, Jacquemart D, Perevalov VI, Perrin A, Shine KP, Smith MAH, Tennyson J, Toon GC, Tran H, Tyuterev VG, Barbe A, Császár AG, Devi VM, Furtenbacher T, Harrison JJ, Hartmann JM, Jolly A, Johnson TJ, Karman T, Kleiner I, Kyuberis AA, Loos J, Lyulin OM, Massie ST, Mikhailenko SN, Moazzen-Ahmadi N, Müller HSP, Naumenko OV, Nikitin AV, Polyansky OL, Rey M, Rotger M, Sharpe SW, Sung K, Starikova E, Tashkun SA, Auwera JV, Wagner G, Wilzewski J, Wcisło P, Yu S, Zak EJ. The HITRAN 2016 molecular spectroscopic database. J Quant Spectrosc Radiat Transfer 2017;203:3–69. doi:10.1016/j.jqsrt.2017.06.038.

[5] Jacquinet-Husson N, Armante R, Scott NA, Chédin A, Crépeau L, Boutammine C, Bouhdaoui A, Crevoisier C, Capelle V, Boonne C, Poulet-Crovisier N, Barbe A, Benner DC, Boudon V, Brown LR, Buldyreva J, Campargue A, Coudert LH, Devi VM, Down MJ, Drouin BJ, Fayt A, Fittschen C, Flaud JM, Gamache RR, Harrison JJ, Hill C, Hodnebrog O, Hu SM, Jacquemart D, Jolly A, Jiménez E, Lavrentieva NN, Liu AW, Lodi L, Lyulin OM, Massie ST, Mikhailenko S, Müller HSP, Naumenko OV, Nikitin A, Nielsen CJ, Orphal J, Perevalov VI, Perrin A, Polovtseva E, Predoi-Cross A, Rotger M, Ruth AA, Yu SS, Sung K, Tashkun SA, Tennyson J, Tyuterev VG, Auwera JV, Voronin BA, Makie A. The 2015 edition of the GEISA spectroscopic database. J Mol Spectrosc 2016;327:31–72. doi:10.1016/j.jms.2016.06.007.

[6] Derzi ARA, Furtenbacher T, Yurchenko SN, Tennyson J, Császár AG. MARVEL analysis of the measured high-resolution spectra of ^{14}NH$_3$. J Quant Spectrosc Radiat Transfer 2015;161:117–30. doi:10.1016/j.jqsrt.2015.03.034.

[7] Kosterev AA, Tittel FK. Ammonia detection by use of quartz-enhanced photoacoustic spectroscopy with a near-IR telecommunication diode laser. Appl Opt 2004;43:6213–17. doi:10.1364/ao.43.006213.

[8] Claps R, Englich FV, Leleux DP, Richter D, Tittel FK, Curl RF. Ammonia detection by use of near-infrared diode-laser-based overtone spectroscopy. Appl Optics 2001;40:4387–94. doi:10.1364/ao.40.004387.

[9] Webber ME, Baer DS, Hanson RK. Ammonia monitoring near 15 μm with diode-laser absorption sensors. Appl Opt 2001;40:2031–42. doi:10.1364/ao.40.002031.

[10] Yurchenko SN, Barber RJ, Yachmenev A, Thiel W, Jensen P, Tennyson J. A variationally computed T=300 K line list for NH$_3$. J Phys Chem A 2009;113:11845–55. doi:10.1021/jp9029425.

[11] Yurchenko SN, Barber RJ, Tennyson J. A variationally computed hot line list for NH$_3$. Mon Not R Astron Soc 2011;413:1828–34. doi:10.1111/j.1365-2966.2011.18261.x.

[12] Huang X, Schwenke DW, Lee TJ. Rovibrational spectra of ammonia. I. Unprecedented accuracy of a potential energy surface used with nonadiabatic corrections. J Chem Phys 2011;134:044320. doi:10.1063/1.3541351.

[13] Huang X, Schwenke DW, Lee TJ. Rovibrational spectra of ammonia. II. Detailed analysis, comparison, and prediction of spectroscopic assignments for ^{14}NH$_3$, ^{15}NH$_3$, and ^{14}ND$_3$. J Chem Phys 2011;134:044321. doi:10.1063/1.3541352.

[14] Sung K, Brown LR, Huang X, Schwenke DW, Lee TJ, Coy SL, Lehmann KK. Extended line positions, intensities, empirical lower state energies and quantum assignments of NH$_3$ from 6300 to 7000 cm^{-1}. J Quant Spectrosc Radiat Transfer 2012;113:1066–83. doi:10.1016/j.jqsrt.2012.02.037.

[15] Huang X., Lee T.J.. HSL-pre3 energies list, visited 30/05/2018. 2013. URL huang.seti.org/NH3/HSL-Pre3/14NH3J=0-10.Levels.

[16] Yurchenko SN, Barber RJ, Tennyson J, Thiel W, Jensen P. Towards efficient refinement of molecular potential energy surfaces: ammonia as a case study. J Mol Spectrosc 2011;268:123–9. doi:10.1016/j.jms.2011.04.005.

[17] Polyansky OL, Ovsyannikov RI, Kyuberis AA, Lodi L, Tennyson J, Yachmenev A, Yurchenko SN, Zobov NF. Calculation of rotation-vibration energy levels of the ammonia molecule based on an ab initio potential energy surface. J Mol Spectrosc 2016;327:21–30. doi:10.1016/j.jms.2016.08.003.

[18] Xu LH, Liu Z, Yakovlev I, Tretyakov MY, Lees RM. External cavity tunable diode laser NH$_3$ spectra in the 1.5 μm region. Infrared Phys Technol 2004;45:31–45.

[19] Li L, Lees RM, Xu LH. External cavity tunable diode laser spectra of the $\nu_1 + 2\nu_4$ stretch-band combination bands of ^{14}NH$_3$ and ^{15}NH$_3$. J Mol Spectrosc 2007;243:219–26.

[20] Lees RM, Li L, Xu LH. New VISTA on ammonia in the 1.5 μm region: assignments for the $\nu_3 + 2\nu_4$ bands of ^{14}NH$_3$ and ^{15}NH$_3$ by isotopic shift labeling. J Mol Spectrosc 2008;251:241–51.

[21] Barton EJ, Yurchenko SN, Tennyson J, Béguier S, Campargue A. A near infrared line list for NH$_3$: analysis of a kitt peak spectrum after 35 years. J Mol Spectrosc 2016;325:7–12. doi:10.1016/j.jms.2016.05.001.

[22] Barton EJ, Polyansky OL, Yurchenko SN, Tennyson J, Civis S, Ferus M, Hargreaves R, Ovsyannikov I, Kyuberis AA, Zobov NF, Béguier S, Campargue A. Absorption spectra of ammonia near 1 μm. J Quant Spectrosc Radiat Transfer 2017;203:392–7. doi:10.1016/j.jqsrt.2017.03.042.

[23] Zobov NF, Coles PA, Ovsyannikov RI, Kyuberis AA, Hargreaves RJ, Bernath PF, Yurchenko SN, Tennyson J, Polyansky OL. Analysis of the red and green optical absorption spectrum of gas phase ammonia. J Quant Spectrosc Radiat Transfer 2018;209:224–31. doi:10.1016/j.jqsrt.2018.02.001.

[24] Polyansky OL, Zobov NF, Viti S, Tennyson J, Bernath PF, Wallace L. K band spectrum of water in sunspots. Astrophys J 1997;489:L205–8.

[25] Coy SL, Lehmann KK. Rotational structure of ammonia NH stretch overtones: five and six quanta bands. J Chem Phys 1986;84:5239–49.

[26] Lehmann KK, Coy SL. Spectroscopy and intramolecular dynamics of highly excited vibrational states of NH$_3$. J Chem Soc Faraday Trans II 1988;84:1389–406.

[27] Coy SL, Lehmann KK. Modeling the rotational and vibrational structure of the i.r. optical spectrum of NH$_3$. Spectrochim Acta 45A 1989;47–56.

[28] Yachmenev A, Yurchenko SN. Automatic differentiation method for numerical construction of the rotational-vibrational hamiltonian as a power series in the curvilinear internal coordinates using the eckart frame. J Chem Phys 2015;143:014105. doi:10.1063/1.4923039.

[29] Yurchenko SN, Thiel W, Jensen P. Theoretical ROVibrational energies (TROVE): a robust numerical approach to the calculation of rovibrational energies for polyatomic molecules. J Mol Spectrosc 2007;245:126–40. doi:10.1016/j.jms.2007.07.009.

[30] Noumerov BV. A method of extrapolation of perturbations. Mon Not R Astron Soc 1924;84:592–602. doi:10.1093/mnras/84.8.592.

[31] Cooley JW. An improved eigenvalue corrector formula for solving the Schrödinger equation for central fields. Math Comp 1961;15:363–74. doi:10.1090/S0025-5718-1961-0129566-X.

[32] Yurchenko SN, Yachmenev A, Ovsyannikov RI. Symmetry-adapted rovibrational basis functions for variational nuclear motion calculations: Trove approach. J Chem Theory Comput 2017;13:4368–81. doi:10.1021/acs.jctc.7b00506.

[33] Yurchenko SN, Carvajal M, Jensen P, Lin H, Zheng JJ, Thiel W. Rotation-vibration motion of pyramidal XY$_3$ molecules described in the Eckart frame: theory and application to NH$_3$. Mol Phys 2005;103:359–78. doi:10.1080/00268970541233151725S.

[34] Mátyus E, Czakó G, Császár AG. Toward black-box-type full- and reduced-dimensional variational (ro)vibrational computations. J Chem Phys 2009;130:134112. doi:10.1063/1.3076742.

[35] Furtenbacher T, Császár AG, Tennyson J. MARVEL: measured active rotational-vibrational energy levels. J Mol Spectrosc 2007;245:115–25. doi:10.1016/j.jms.2007.07.005.

[36] Furtenbacher T., Coles P.A., Tennyson J., Császár A.G.. Updated MARVEL energy levels for ammonia. J Quant Spectrosc Radiat Transfer, To be submitted.

[37] Schryber JH, Polyansky OL, Jensen P, Tennyson J. On the spectroscopically determined potential energy surfaces for the electronic ground states of NO$_2$ and H$_2$O. J Mol Spectrosc 1997;185:234–43.

[38] Giver LP, Miller JH, Boese RW. A laboratory atlas of the $5\nu_1$ NH3 absorption band at 6475 Å with applications to Jupiter and Saturn. Icarus 1975;25:34–48. doi:10.1016/0019-1035(75)90187-6.

[39] Yurchenko SN, Carvajal M, Jensen P, Herregodts F, Huet TR. Potential parameters of PH$_3$ obtained by simultaneous fitting of ab initio data and experimental vibrational band origins. Chem Phys 2003;290:59–67.

[40] Watson JKG. Robust weighting in least-square fits. J Mol Spectrosc 2003;219:326–8.

[41] Rajamäki T, Kallay M, Noga J, Valiron P, Halonen L. High excitations in coupled-cluster series: vibrational energy levels of ammonia. Mol Phys 2004;102:2297–310. doi:10.1080/00268970412331292759.

[42] Pawłowski F, Jørgensen P, Olsen J, Hegelund F, Helgaker T, Gauss J, Bak KL, Stanton JF. Molecular equilibrium structures from experimental rotational constants and calculated vibration–rotation interaction constants. J Chem Phys 2002;116:6482–96. doi:10.1063/1.1459782.

[43] Landolt H, Börnstein I. Numerical data and functional relationships in science and technology group II volume 7. New York: Springer-Verlag; 1976.

[44] Sung K, Brown LR, Huang X, Schwenke DW, Lee TJ, Coy SL, Lehmann KK. Extended line positions, intensities, empirical lower state energies and quantum assignments of $^{14}NH_3$ from 6300 to 7000 cm^{-1}. J Quant Spectrosc Radiat Transfer 2012;113:1066–83. doi:10.1016/j.jqsrt.2012.02.037.

[45] Mizus II, Kyuberis AA, Zobov NF, Makhnev VY, Polyansky OL, Tennyson J. High accuracy water potential energy surface for the calculation of infrared spectra. Phil Trans Royal Soc London A 2018;376:20170149. doi:10.1098/rsta.2017.0149.

[46] Yurchenko SN, Thiel W, Carvajal M, Lin H, Jensen P. Rotation-vibration motion of pyramidal XY_3 molecules described in the eckart frame: the calculation of intensities with application to NH_3. Adv Quant Chem 2005;48:209–38. doi:10.1016/S0065-3276(05)48014-4.

[47] Yurchenko S.N., Al-Refaie A.F., Tennyson J.. ExoCross: a general program for generating spectra from molecular line lists. Astron Astrophys. **614**, 2018. A131, doi: 10.1051/0004-6361/201732531.

[48] Yurchenko SN, Carvajal M, Lin H, Zheng JJ, Thiel W, Jensen P. Dipole moment and rovibrational intensities in the electronic ground state of NH_3: bridging the gap between ab initio theory and spectroscopic experiment. J Chem Phys 2005;122:104317. doi:10.1063/1.1862620.

[49] Lodi L, Tennyson J, Polyansky OL. A global, high accuracy ab initio dipole moment surface for the electronic ground state of the water molecule. J Chem Phys 2011;135:034113. doi:10.1063/1.3604934.

[50] Polyansky OL, Bielska K, Ghysels M, Lodi L, Zobov NF, Hodges JT, Tennyson J. High accuracy CO_2 line intensities determined from theory and experiment. Phys Rev Lett 2015;114:243001. doi:10.1103/PhysRevLett.114.243001.

[51] Werner HJ, Knowles PJ, Knizia G, Manby FR, Schütz M. Molpro: a general-purpose quantum chemistry program package. WIREs Comput Mol Sci 2012;2:242–53. doi:10.1002/wcms.82.

[52] Sousa-Silva C, Hesketh N, Yurchenko SN, Hill C, Tennyson J. High temperature partition functions and thermodynamic data for ammonia and phosphine. J Quant Spectrosc Radiat Transfer 2014;142:66–74. doi:10.1016/j.jqsrt2014.03.012.

[53] Al-Refaie AF, Tennyson J, Yurchenko SN. GPU accelerated INtensities MPI (GAIN-MPI): a new method of computing Einstein-*A* coefficients. Comput Phys Commun 2017;214:216–24. doi:10.1016/j.cpc.2017.01.013.

[54] Tennyson J, Yurchenko SN, Al-Refaie AF, Barton EJ, Chubb KL, Coles PA, Diamantopoulou S, Gorman MN, Hill C, Lam AZ, Lodi L, McKemmish LK, Na Y, Owens A, Polyansky OL, Rivlin T, Sousa-Silva C, Underwood DS, Yachmenev A, Zak E. The exomol database: molecular line lists for exoplanet and other hot atmospheres. J Mol Spectrosc 2016;327:73–94. doi:10.1016/j.jms.2016.05.002.

[55] Vander Auwera J., Vanfleteren T.. Line positions and intensities in the 7400–8600 cm^{-1} region of the ammonia spectrum. Mol Phys. doi: 10.1080/00268976.2018.1467054.

[56] Czinki E., Furtenbacher T., Császár A.G.. SpectropediaVisited 01/11/2017. URL respecth.chem.elte.hu:8080/spectro2017D.

[57] Irwin P.G.J., Bowles N., Braude A.S., Garland R., Coles P.A., Yurchenko S.N., Tennyson J., Calcutt S.. Analysis of gaseous ammonia (NH_3) absorption in the visible spectrum of Jupiter - Update, Icarus, submitted.